

Special Section:

Recent Progresses in Oceanography and Air-Sea Interactions in Southeast Asian Archipelago

Key Points:

- Hydrographic investigation and glider data show the transport of subsurface saline Kuroshio water into the northern South China Sea
- The eddy-induced transport of saline Kuroshio water occurs in two stages with different dominant transport mechanisms
- A diagnosis of salinity budget confirms that the eddy flow advection plays a major role in salinity transport in the second stage




Correspondence to:L. Zeng,
zenglili@scsio.ac.cn**Citation:**Yang, Y., Wang, D., Wang, Q., Zeng, L., Xing, T., He, Y., et al. (2019). Eddy-induced transport of saline Kuroshio water into the northern South China Sea. *Journal of Geophysical Research: Oceans*, 124. <https://doi.org/10.1029/2018JC014847>

Received 11 DEC 2018

Accepted 18 AUG 2019

Accepted article online 27 AUG 2019

Eddy-Induced Transport of Saline Kuroshio Water Into the Northern South China Sea

Yikai Yang^{1,2}, Dongxiao Wang¹ , Qiang Wang¹ , Lili Zeng¹ , Tao Xing^{2,3}, Yunkai He¹, Yeqiang Shu¹, Ju Chen¹, and Yinxia Wang^{4,5}

¹State Key Laboratory of Tropical Oceanography (LTO), South China Sea Institute of Oceanology, Chinese Academy of Sciences, Guangzhou, China, ²University of Chinese Academy of Sciences, Beijing, China, ³MLR Key Laboratory of Marine Mineral Resources, Guangzhou Marine Geological Survey, Guangzhou, China, ⁴South China Sea Institute of Planning and Environmental Research, State Oceanic Administration, Guangzhou, China, ⁵Key Laboratory of Technology for Safeguarding of Maritime Rights and Interests and Application, SOA, Guangzhou, China

Abstract To better understand eddy-induced heat and salt transport, a targeted joint hydrographic investigation focusing on an anticyclonic eddy was carried out in July 2017 in the northern South China Sea. In situ and satellite observations together with Hybrid Coordinate Ocean Model (HYCOM) output show the transport of subsurface saline Kuroshio water into the northern South China Sea by an anticyclonic eddy. Subsurface high-salinity cores are consistent with the anticyclonic eddy centers. The transport of saline Kuroshio water occurs in two stages accompanied by eddy shedding. First, saline Kuroshio water is trapped within the anticyclonic eddy at its generation location. Then, although the salinity within the eddy gradually weakens as the eddy carries the saline water westward, the quantity of saline water (>34.70 psu) shows a sharp increase, dominated by eddy-induced salinity advection. A diagnosis of the salinity budget further confirms that the contribution of eddy flow advection is greater than that of mean flow advection. The saline Kuroshio water is trapped and conveyed in this anticyclonic eddy, providing vital evidence and important implications for eddy-induced salt transport and water exchange.

1. Introduction

The South China Sea (SCS) is the largest semienclosed marginal sea in the tropical ocean. Its northern basin, the northern SCS (NSCS), is surrounded by Hainan Island, Mainland China, Taiwan Island, and Vietnam and is connected to the western Pacific via the Luzon Strait and to the East China Sea via the Taiwan Strait. The SCS Throughflow acts as a heat and salt conveyor belt to bring large amounts of warm and saline Kuroshio water into the basin through the Luzon Strait (Gordon et al., 2012; Jia & Liu, 2004; Liu et al., 2012; Qu et al., 2006; Wang et al., 2006). The heat and salt exchange significantly affects the heat and salt balances in the SCS (Chen et al., 2012; Chen et al., 2017; Xiao et al., 2017; Zeng et al., 2014, 2018; Zeng, Wang, Chen, et al., 2016).

Mesoscale eddies are found throughout the SCS, especially in the NSCS (Chen, 2010; Huang, 1992; Su et al., 1999; Wang et al., 2003; Wang et al., 2008; Xiu et al., 2010; Zhang, 1994). Previous research found the complicated topography and the Kuroshio eddy shedding process to be two major causes of eddy activity in the NSCS (Hetland et al., 1999; Hurlburt & Thompson, 1980; Li et al., 1998; Sangrà et al., 2005). The complex island topography also has a major effect on the generation and propagation of eddies in the NSCS, especially that of the neighboring Dongsha and Xisha Islands (Wang et al., 2014). The islands contribute greatly to eddy development (Evans et al., 1985), propagation (Schultz Tokos et al., 1994; Waterman, 2009), and dissipation (Cheney & Richardson, 1976; McWilliams & Flierl, 1979). Using singular value decomposition analysis of the covariability between temperature from moorings and satellite altimetry data, Lin et al. (2015) identified two types of mesoscale eddy pattern, one travelling westward from the Luzon Strait and the other travelling southwestward from southwestern Taiwan. Theoretical studies suggest that anticyclonic eddies are shed from Kuroshio intrusions into the SCS that take the form of an anticyclonic loop (Li et al., 1998). Using satellite and hydrological data, Wang et al. (2008) reported cases of anticyclone eddies shedding off from the Kuroshio, while Wang et al. (2000) analyzed mean XBT data and pointed out that the baroclinic instability of the Kuroshio may contribute to the generation of mesoscale eddies in the NSCS. Sheu et al. (2010) suggested that the fate of eddies (i.e., whether they freely propagate westward through the Luzon Strait into the SCS) depends mainly on the strength and path of the Kuroshio.

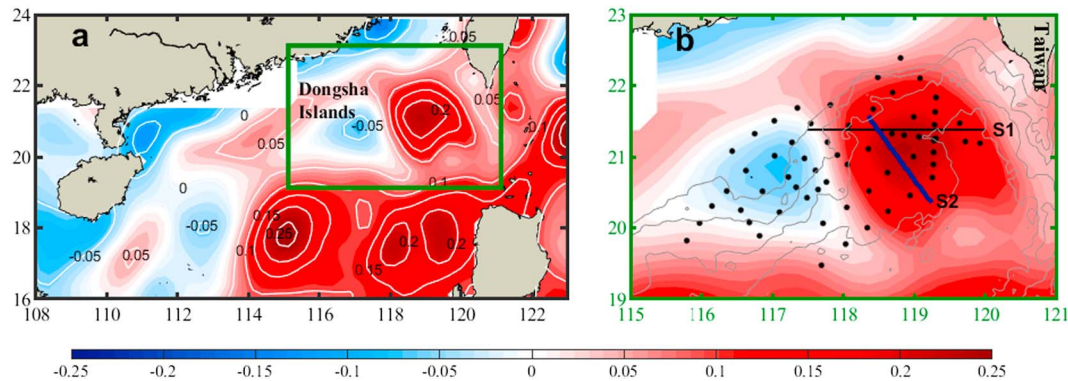


Figure 1. Mean sea level anomaly (shading; unit: m) over the northern South China Sea within the lifespan of the anticyclonic eddy, from 13 to 22 July 2017. (a) The green box highlights the region of the anticyclonic eddy and cruise, shown in detail in (b), where shipboard measurement sites of expendable conductivity-temperature-depth recorders during the cruise are indicated by black dots. The black line (S1) is a zonal section crossing the latitude of the mean eddy center. The blue line (S2) is the glider route from 15 to 21 July. The gray lines are the 500-, 1,000-, 2,000-, and 3,000-m isobaths.

Many studies have demonstrated that eddy-induced transport can be comparable with that of the large-scale circulation (Bryan, 1996; Dong et al., 2014; Jayne & Marotzke, 2002; Volkov et al., 2008; Zhang et al., 2014). Considering the vigor of the eddies shed by the Kuroshio into the NSCS, eddy-induced transport is likely to be important for heat and salt intrusion. Dong et al. (2014) suggested that temperature and salinity anomalies inside individual eddies tend to move with eddies because of advective trapping of interior water parcels. Even though the potential importance of eddy heat and salt transport has been well recognized, the structure and evolution of eddies, together with the mechanisms of eddy transport processes in the NSCS, are still unclear. An increase in the number of in situ measurements and the development of high-resolution numerical models enable a more intensive study of eddy transport processes. In particular, several cruises have captured examples of classic eddies in the SCS in recent years. For example, a field cruise in August 2010 provided detailed characteristics of an exceptional anticyclonic eddy (AE) near the Xisha Islands (Chu et al., 2014). Several long-lived AEs along 18°N and their detailed evolution were described by cruises in August 2007 and 2012 (Nan et al., 2011).

To further investigate eddy-induced transport processes, a targeted joint hydrographic investigation was conducted during summer 2017. In this paper, we focus on analyzing the saline water transported to the NSCS by an AE. The remainder of this paper is organized as follows. Section 2 describes the in situ and satellite data, model output data, and methods. Section 3 presents the observed characteristics of the eddy and observed saline water intrusion. Section 4 shows the characteristics, evolution, and dynamic diagnosis of eddy saline water transport processes. Finally, a discussion and summary are given in sections 5 and 6, respectively.

2. Data and Methods

2.1. In Situ and Satellite Datasets, and Model Output

The July 2017 cruise field covered the area 19–22.5°N and 115.5–120°E, from 13 to 22 July (Figure 1). After quality control, 62 expendable conductivity-temperature-depth recorder (XCTD) profiles were selected and used in this study. The observation accuracies of the XCTD are ± 0.03 S/m for electric conductivity, $\pm 0.02^\circ\text{C}$ for temperature, and $\pm 2\%$ for depth, respectively. The vertical resolution of the XCTD observation was 1 m. We also used several sets of data from a Sea-Wing underwater glider developed by the Shenyang Institute of Automation, Chinese Academy of Sciences (Shu et al., 2018). All of the gliders were equipped with a Slocum Glider Payload conductivity-temperature-depth (CTD) sensor produced by Sea-Bird Electronics (SBE) in the United States. The observation accuracies of the CTD are ± 0.0003 S/m for electric conductivity, $\pm 0.002^\circ\text{C}$ for temperature, and $\pm 0.1\%$ for pressure, respectively. In addition to cruise observations, we use the climatological mean gridded South China Sea Physical Oceanographic Dataset (SCSPOD14), derived from in situ measurements during 1919–2014 (Zeng, Wang, Chen, et al., 2016).

The daily sea level anomaly (SLA) and surface currents from the French Archiving, Validation and Interpretation of Satellite Oceanographic (AVISO) data project from May 2017 to October 2017 have been

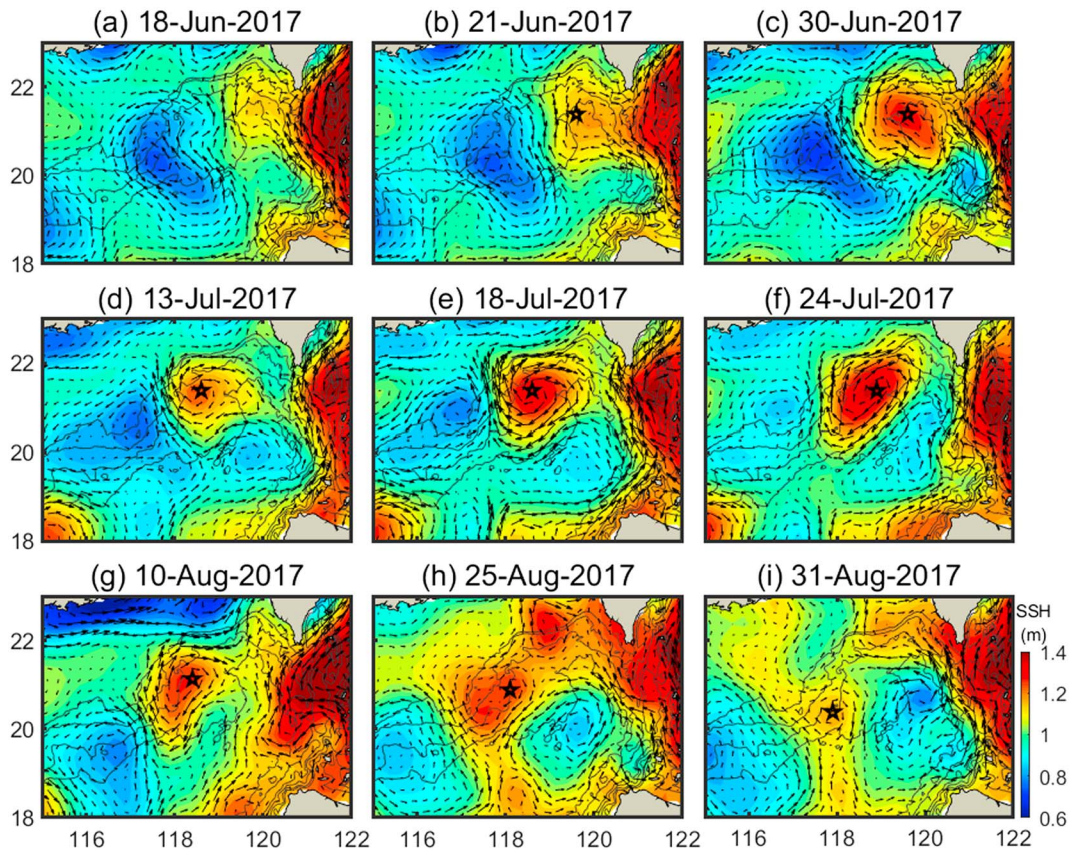


Figure 2. Evolution of the anticyclonic eddy center detected by satellite sea surface height (shading; unit: m) and geostrophic current (vectors; unit: m/s) for (a) 18 June, (b) 21 June, (c) 30 June, (d) 13 July, (e) 18 July, (f) 24 July, (g) 10 August, (h) 25 August, and (i) 31 August. Eddy centers are marked by black stars. The black lines are the 500-, 1,000-, 2,000-, and 3,000-m isobaths.

used to detect the evolution of this AE. The merged altimetry data are a combination of Jason, TOPEX/Poseidon, Envisat, GFO, ERS, and Geosat altimeters, with $1/4^\circ$ resolution.

To examine the importance of eddy-induced salt transport, daily ocean current, temperature, and salinity data with $1/12^\circ \times 1/12^\circ$ resolution from the Hybrid Coordinate Ocean Model (HYCOM) data are used to reconstruct the vertical structure of the eddy and the eddy-induced high-salinity water transport. As part of the Global Ocean Data Assimilation Experiment, the HYCOM consortium developed and evaluated a

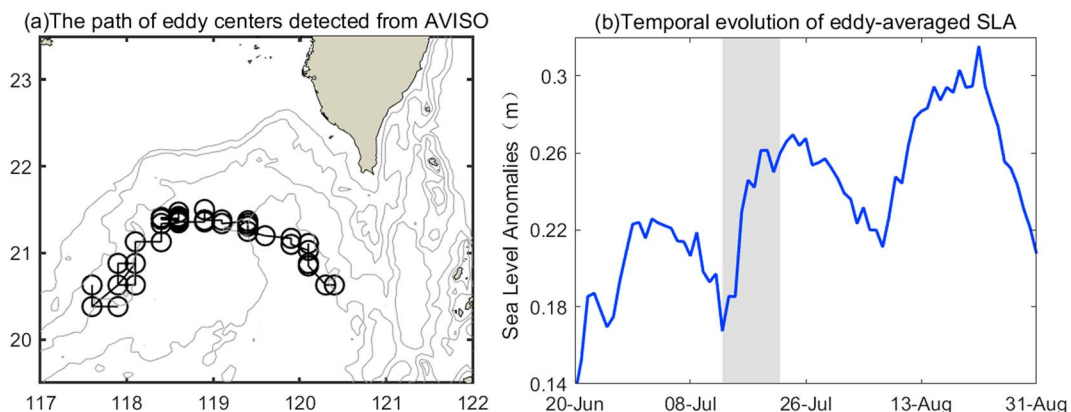


Figure 3. (a) Path of the eddy center detected from Archiving, Validation and Interpretation of Satellite Oceanographic (AVISO) data. The gray lines are the 500-, 1,000-, 2,000-, and 3,000-m isobaths. (b) Temporal evolution of eddy-averaged sea level anomaly (SLA; unit: m). The cruise period, 13 to 22 July, is shaded gray.

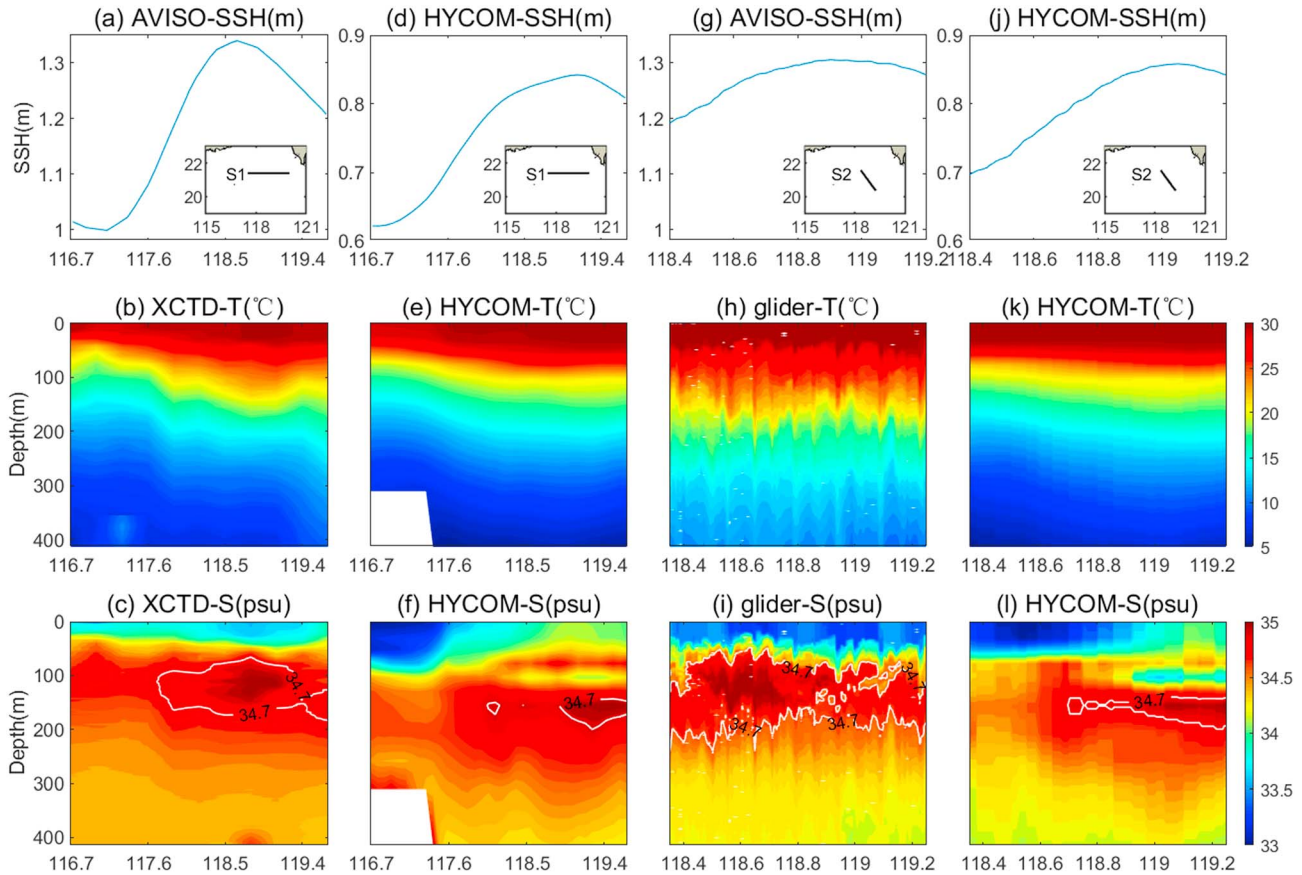


Figure 4. (a) Zonal sea surface height (unit: m) along the latitude of mean eddy center, marked as black line S1 in Figure 1b. (b) Zonal averaged temperature (unit: °C) distribution along the latitude of mean eddy center observed by expendable conductivity-temperature-depth recorder (XCTD). (c) Zonal averaged salinity (unit: psu) distribution along the latitude of mean eddy center observed by XCTD. The white contours show the 34.70-psu isohaline. (d–f) Same as (a)–(c) but for Hybrid Coordinate Ocean Model (HYCOM) data. (g–i) Glider data along the blue line S2 in Figure 1b. (j–l) Same as (g)–(i) but for HYCOM data. Locations of the measurement sections are shown in the inset (a, d, g, and j).

data-assimilative hybrid isopycnal-sigma-pressure (generalized) coordinate ocean model. The model was initialized using temperature and salinity from the 1/4° Generalized Digital Environmental Model climatology and forced with data from the Navy Operational Global Atmospheric Prediction System (Chassignet et al., 2007).

2.2. Winding-Angle Eddy Tracking Method

The Winding-Angle (W-A; Sadarjoen & Post, 2000) method is used to identify and track the AE in satellite altimetry data; this method has been widely used in mesoscale eddy studies in the SCS (Chen et al., 2011; Chu et al., 2014). Maximal (minimal) sea level anomalies are first identified in a 4 × 4 grid-point moving window, then closed streamlines are selected by computing wind angle, and clustered to different eddies.

2.3. Intensity of Saline Kuroshio Water Intrusion Within an Eddy

The intensity of saline Kuroshio water trapped and transported within the AE is represented by an index of saline Kuroshio water intrusion within an eddy, I_s , which is defined as the area integral of high-salinity water within the eddy divided by the area occupied by the saline water, that is, the average salinity over high-salinity areas:

$$I_s = \frac{1}{\Omega} \int_{\Omega} S d\Omega \quad (1)$$

where S is salinity and Ω is the area occupied by water saltier than 34.70 psu within the eddy. Following previous studies (Qu et al., 2000; Zeng, Wang, Xiu, et al., 2016; Zeng, Wang, Chen, et al., 2016), 34.70 psu is

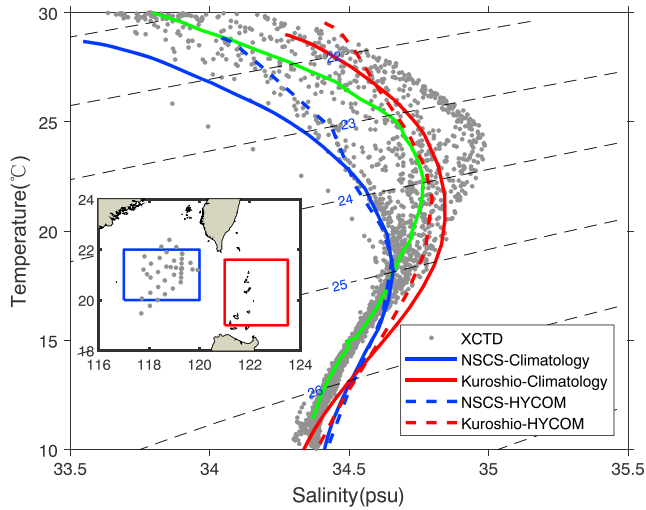


Figure 5. *T-S* diagram (gray dots) and averaged *T-S* curve (green) based on expendable conductivity-temperature-depth recorder (XCTD) observations within the eddy. The blue and red lines are the averaged *T-S* curves for the northern South China Sea (blue box) and Kuroshio area (red box), respectively, based on climatology data. The blue and red dashed lines are the corresponding curves for Hybrid Coordinate Ocean Model (HYCOM) data. The boxes and stations are shown in the inset.

chosen as the criterion to distinguish between SCS water and Kuroshio water. The area of saline water is obtained using the grid points occupied by saline Kuroshio water, which are recorded in a three-dimensional array of $2^\circ \times 2^\circ$ around the eddy center. Larger I_s means that more salinity Kuroshio water is trapped and conveyed within the eddy.

2.4. Simplified Subsurface Salt Balance

To investigate the dynamics of eddy-induced saline Kuroshio intrusion, the simplified salinity equation is diagnosed:

$$\underbrace{S_t}_{S \text{ tendency}} = \underbrace{-\nabla \cdot (\bar{\mathbf{u}}S) - \nabla \cdot (\mathbf{u}'S)}_{\text{Horizontal advection}} + \underbrace{\varepsilon}_{\text{Residual}} \quad (2)$$

where the terms are (from left to right) salinity tendency, horizontal advection, and a residual that contains entrainment, detrainment, diffusion, and other less important factors. Here S_t is the tendency of salinity trapped and transported with the eddy, and $\mathbf{u}S$ is the horizontal salt flux. $\nabla = \partial_x i + \partial_y j$ is the Laplace operator. The horizontal advection term contains two components: the mean flow advection ($-\nabla \cdot (\bar{\mathbf{u}}S)$) and eddy flow advection ($-\nabla \cdot (\mathbf{u}'S)$). The mean flow $\bar{\mathbf{u}}$ is a low-pass filtered time series (period longer than 90 days), and the prime indicates the remaining (eddy) flow. According to previous studies (Lee et al., 1997, 2007), the total transport of a water mass within an isopycnal layer consists mainly of the

transport by the time-mean velocity, the transport by eddy advection, and eddy diffusion. In this study, the residual term ε containing the diffusion term is omitted.

3. Observed Eddy-Induced Intrusion of Saline Kuroshio Water

The sea surface height (SSH) field clearly demonstrates an AE being shed from the Kuroshio (Figure 2). In mid-to-late June, the Kuroshio loop entered the SCS (Figure 2a). The Kuroshio extended west of 119°E and then curved clockwise back to the Pacific through the northern Luzon Strait. In late June, an AE formed within the Kuroshio loop and a cyclonic eddy formed to its west (Figure 2b). The AE was shed from the Kuroshio at the end of June and gradually decayed in the following two weeks (Figure 2d). Then, the AE strengthened again in mid-July and turned to propagate westward (Figures 2e and 2f). This period of rapid growth was well captured by our investigation cruise. In late July, the eddy weakened again and turned to strengthen a third time in early August. The eddy then dissipated rapidly as it hit the Dongsha slope (Figures 2h and 2i). Subsequently, it moved southward and merged with another AE to its south. In this study, we focus on the evolution of the eddy from mid-June to late August.

To better understand the propagation of the eddy, the W-A eddy tracking procedure was used to identify and track the eddy. The detected eddy centers during the eddy lifespan show a propagation path along the slope (Figure 3a). The average value of SLA evolution within the eddy (defined as a $1^\circ \times 1^\circ$ bin around the eddy center) is also calculated (Figure 3b). Active periods in mid-July (with the secondary maximum SLA of 26 cm) and mid-August (with a maximum SLA of 29 cm) are consistent with the growth cycle shown in Figure 2.

The average shape and dynamical parameters of this AE are also calculated. Once the closed streamlines are determined by W-A method, the mean radius is available and thus other properties. Assuming geostrophic balance and isotropy, eddy kinetic energy (EKE) maps are computed using the formula $\text{EKE} = \frac{1}{2} (U_g'^2 + V_g'^2)$. The geostrophic velocity anomalies are deduced from SLA maps using the geostrophic approximation, $U_g' = -\frac{g}{f} \frac{\partial \eta'}{\partial y}$ and $V_g' = -\frac{g}{f} \frac{\partial \eta'}{\partial x}$, where U_g' and V_g' are the zonal and meridional components of the geostrophic velocity anomaly, respectively; g is the gravitational constant; η' is the SLA, and f is the Coriolis parameter. The vorticity for an eddy is averaged within the eddy and calculated as $\Omega = \frac{\partial V_g'}{\partial x} - \frac{\partial U_g'}{\partial y}$,

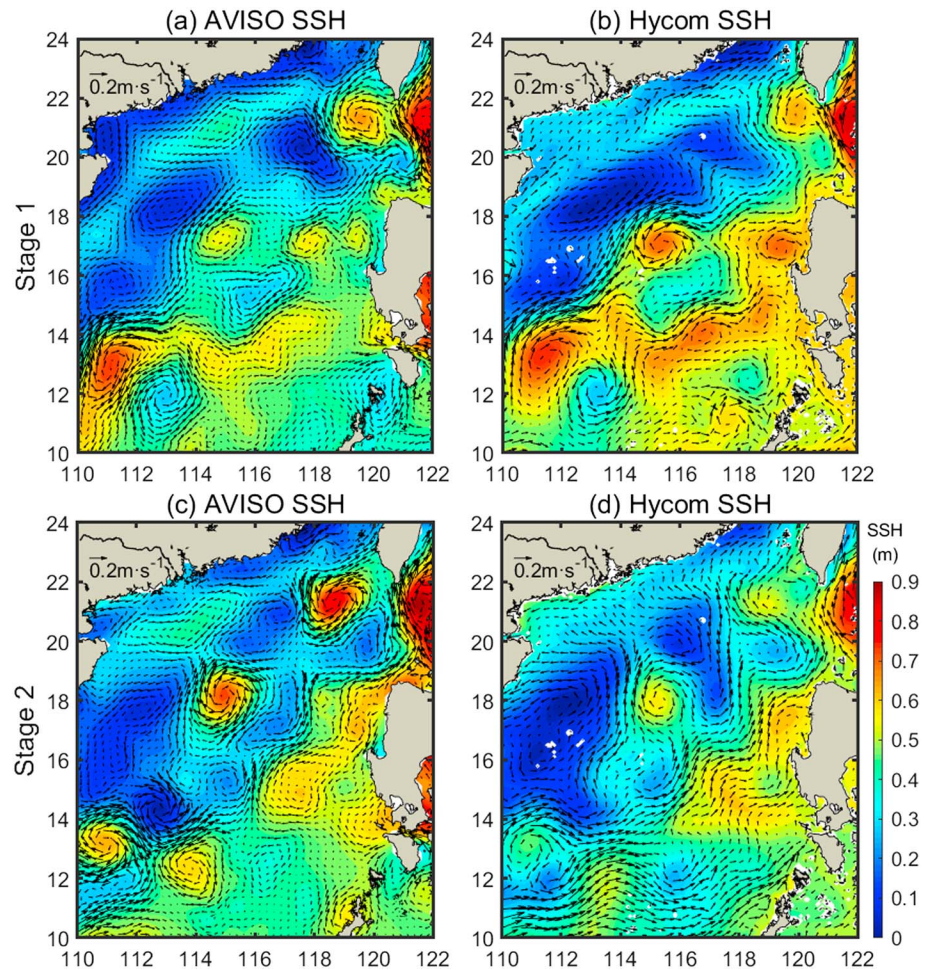


Figure 6. Mean sea surface height (SSH, shading; unit: m) and surface currents (vectors; unit: m/s) from 20 June to 8 July (stage 1) from (a) Archiving, Validation and Interpretation of Satellite Oceanographic (AVISO) data and (b) Hybrid Coordinate Ocean Model (HYCOM) data. (c) and (d) Same as (a) and (b) but from 13 to 29 July (stage 2).

and the divergence as $\nu = \frac{\partial U'_x}{\partial x} + \frac{\partial V'_y}{\partial y}$. The mean radius of the eddy was 1.23×10^2 km, mean kinetic energy was $0.06 \text{ m}^2/\text{s}^2$, mean divergence was $1.83 \times 10^{-9}/\text{s}$, and mean vorticity was $-8.73 \times 10^{-8}/\text{s}$. Over its lifespan, the eddy can be considered a typical SCS mesoscale eddy (Chen, 2010; Xiu et al., 2010). The observed temperature and salinity profiles at the center and edge of the eddy show typical characteristics (Figure 4). Near the eddy center, the warm temperature anomaly is strong at the surface and extends downward (Figures 4b and 4h). However, the salinity structure varies with depth (Figures 4c and 4i). A fresher AE core in the upper layer is underlain by a subsurface maximum-salinity core between 100- and 250-m depth. The salinity in the core is higher than 34.70 psu, which is regarded as typical of a saline Kuroshio water mass originating from the central subtropical Pacific Ocean (Qu, 2000; Li & Wang, 2012; Nan et al., 2015; Zeng, Wang, Xiu, et al., 2016). Note that the glider section S2 (Figure 1b) does not cross the mean eddy center, and so has lower SSH than in section S1, with values ranging from 1.16 to 1.30 m (Figure 4g). The observed profiles agree closely with results from HYCOM data (Figures 4d–4f and 4i–4l), which closely reproduce the characteristics of the subsurface maximum-salinity core and top-down temperature decline even though SSH values are underestimated.

The water mass characteristics of the AE are determined from the XCTD profiles (Figure 5). The typical SCS water is cooler and fresher than the warm and saline Kuroshio water in both the climatology and HYCOM data. The T – S curve of the eddy is much closer to the curve of Kuroshio water, with many subsurface observations saltier than 34.70 psu. Thus, the eddy appears to contain Kuroshio water that is probably

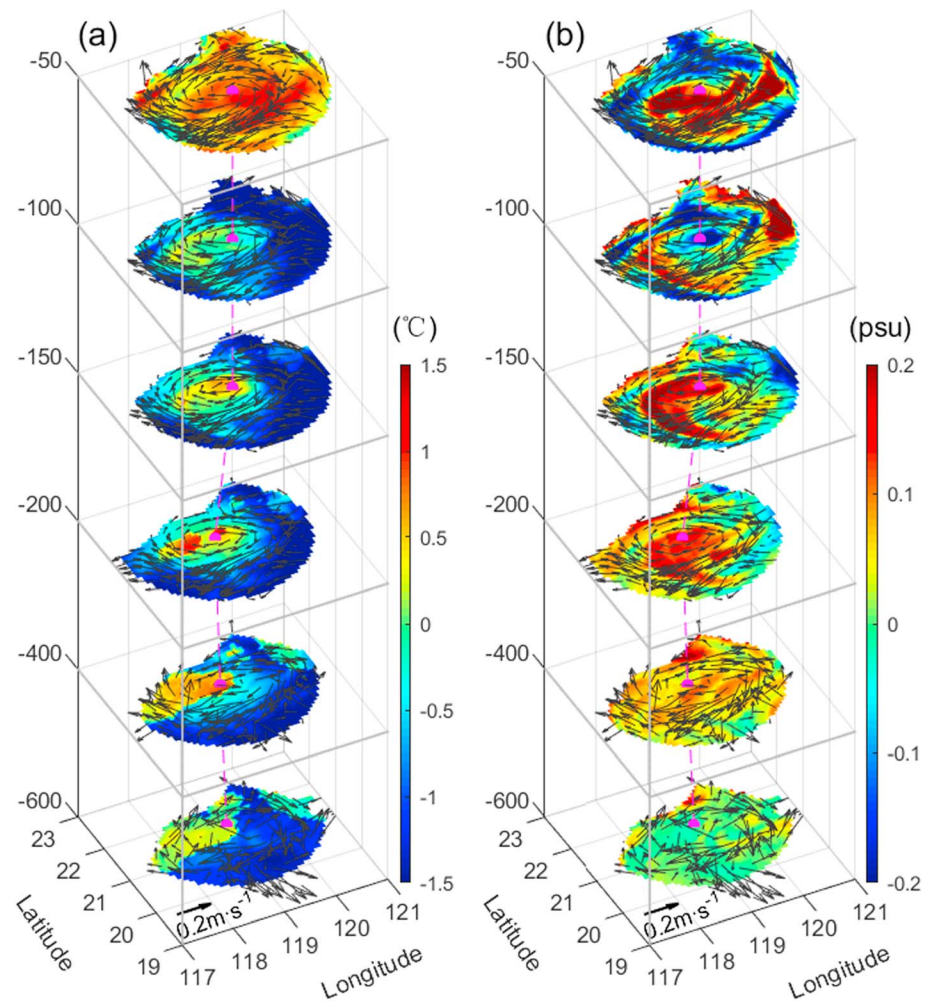


Figure 7. 3-D structures of (a) temperature anomaly (shading; unit: °C) and (b) salinity anomaly (shading; unit: psu) as well as horizontal velocity (vectors; unit: m/s) on 12 July 2017.

conveyed by the eddy itself. This suggests that saline Kuroshio water can be transported into the NSCS by eddy movement. More evidence for this phenomenon and the dynamic processes will be discussed in the following section.

4. Eddy Salt Transport Into the Northern SCS

4.1. Evidence of Eddy Salt Transport

HYCOM output are widely used to study the circulation and water exchange in the NSCS due to the model's high resolution and good simulation skill (Shu et al., 2014; Zeng et al., 2018). A comparison between HYCOM output and the AVISO satellite altimeter data in Figure 6 shows good agreement for the circulation and eddies. Both the pattern and location of the eddy of the present study are well simulated, although the surface height is underestimated by HYCOM. The three-dimensional structure of the eddy on 12 July 2017, as simulated by HYCOM, is shown in Figure 7. The AE decays with depth and weakens rapidly below 500 m. There is a high-salinity core in the subsurface layer, similar to that in the observed vertical profile (Figure 5).

The propagation path of the AE detected from HYCOM is highly consistent with that detected by the satellite altimeter (Figure 8), which validates the simulation of the eddy. We also find that the subsurface high-salinity cores coincide well with the eddy centers mentioned above. Here a high-salinity core is defined as

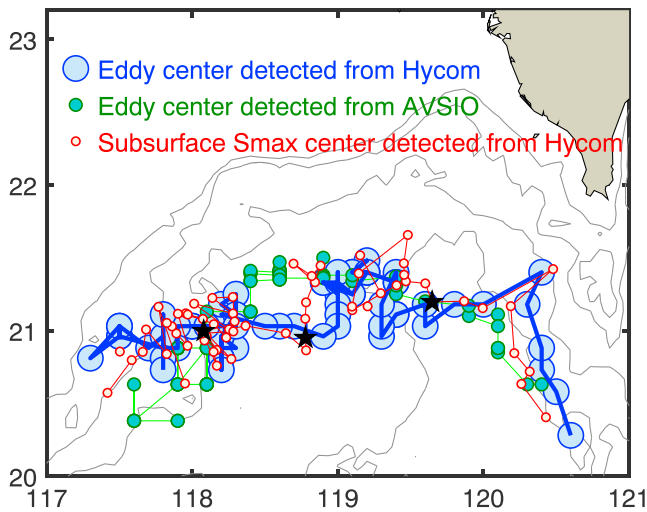


Figure 8. Eddy centers detected from Archiving, Validation and Interpretation of Satellite Oceanographic (AVISO; green dots), Hybrid Coordinate Ocean Model (HYCOM; blue dots), and subsurface high-salinity water cores detected from HYCOM (red dots). The black stars are three typical eddy centers detected from HYCOM on (from east to west) 28 June, 24 July, and 8 August.

the mean location of water mass saltier than 34.70 psu. The close relationship between eddy centers and high-salinity cores confirms the above hypothesis that the AE conveyed the saline Kuroshio water into the NSCS as it propagated.

To show clearly whether high-salinity water is transported by the eddy, three typical snapshots of the eddy are presented in Figure 9. Although the shape of the saline Kuroshio intrusion varies at different times, its maximum core always coincides with the AE center. On 28 June, which is the first snapshot, the AE began to propagate westward. A meridional high-salinity band appeared in the subsurface layer (Figure 9a). The saline Kuroshio intrusion water was mainly limited to within the AE area, suggesting the dominance of the eddy trapping effect. Corresponding to the rising SSH within the eddy, a high-salinity core appeared in the subsurface layer (Figures 9b and 9c). In the second snapshot, on 24 July, the AE propagated westward to about 118.5°E, 21°N (Figure 9d). The saline Kuroshio intrusion water was distributed in a zonal band along the eddy's southern fringe, suggesting the influence of eddy advection. The surface height increased to 0.8 m at the eddy center. Associated with the raised sea surface, a significant high-salinity core appeared within the eddy area (Figures 9e and 9f). For the third snapshot, on 8 August, the eddy continued to propagate westward. The saline Kuroshio intrusion water began to mix away. Although the strength of the eddy and high-salinity water were

weaker than on 24 July, the close relationship between the eddy center and high-salinity core was still obvious (Figures 9h and 9i). These three snapshots clearly show the eddy-induced intrusion of saline Kuroshio water at different times along its westward propagation.

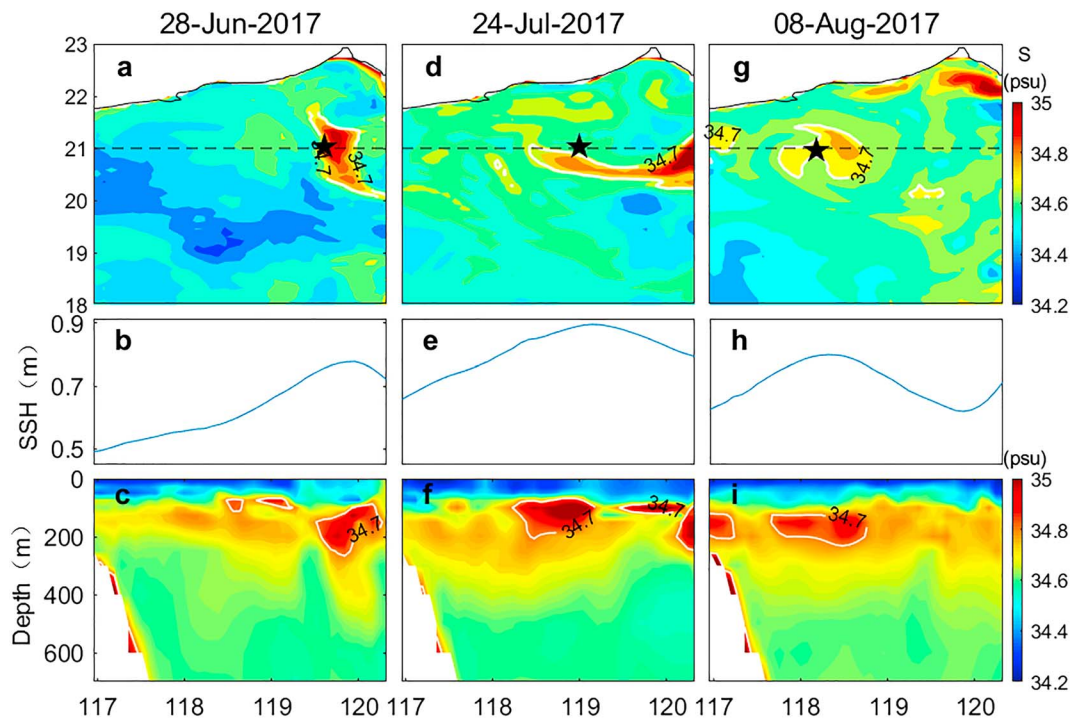


Figure 9. Typical snapshots of (a) the horizontal distribution of salinity in the subsurface layer (at 200-m depth), where the black stars represent eddy centers that are also marked in Figure 8, (b) zonal profiles of sea surface height (unit: m) time series along 21°N, and (c) zonal vertical sections of salinity along 21°N, on 28 June. (d–f) and (g–i) Same as (a)–(c) but for snapshots on 24 July and 8 August, respectively. The white lines show the 34.70-psu isohaline. The dotted lines represent 21°N.

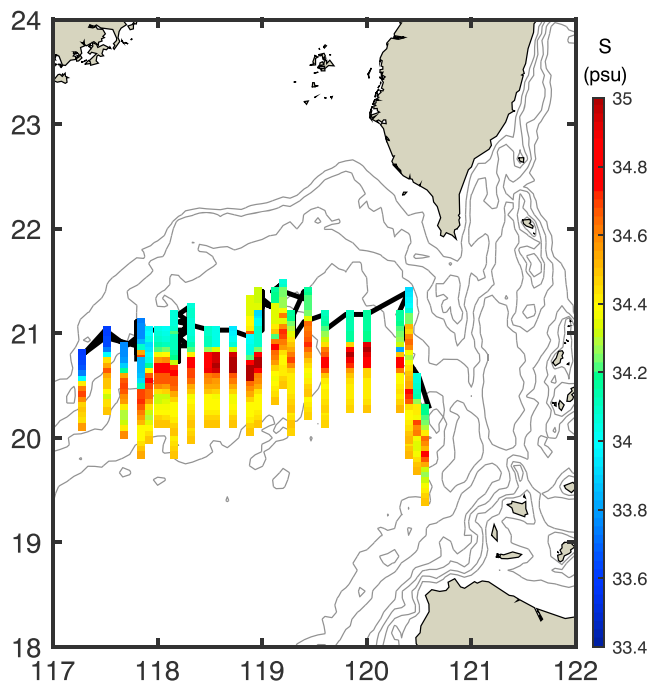


Figure 10. Propagation path of the anticyclonic eddy (black curve) and vertical salinity (shaded column; unit: psu) around the eddy center from the sea surface to 1,000-m depth. The black lines are the 500-, 1,000-, 2,000-, and 3,000-m isobaths.

ity of the eddy, with a peak of 35 psu. Thus, the evolution of eddy high-salinity intensity further confirms that salinity dissipation dominated the first stage, and there was a sharp salinity increase in the second stage.

Details of these two stages are shown in Figure 13. Before the eddy split off, the Kuroshio intrusion brought abundant saline water to the Luzon Strait (Figure 13a). The eddy was generated adjacent to the northwest

In addition to typical snapshots, the time evolution of the vertical salinity structure along the propagation path of the eddy is presented in Figure 10. Note that there is always a high-salinity core in the subsurface layer moving along with the eddy. That is, the typical snapshots and the time-evolution of the high-salinity core with eddy propagation further confirm the eddy transport of high-salinity Kuroshio water into the SCS.

4.2. Two Stages of AE-Induced Intrusion of Saline Kuroshio Water

Having confirmed that the Kuroshio saline water is transported by the eddy, it is important to further investigate the characteristics and dynamics of the eddy transport processes. The evolution of subsurface salinity and eddy centers along 21°N, the main latitude of eddy centers, is shown in Figure 11. The time-longitude distribution of subsurface salinity further confirms the eddy-induced intrusion of saline Kuroshio water. There were two stages in this intrusion process: one around late June and the other in mid-to-late July. The first stage, with northwestward propagation (Figures 2a–2c and 3a), involved a salinity dissipation process. In the second stage, the eddy began to move westward, with a sharp increase in salinity.

The intensity of the eddy-induced intrusion of saline Kuroshio water is quantified using the index I_s (see section 2.3). Consistent with Figure 11, there are two stages of eddy-induced transport (Figure 12). In the first stage, from 20 June to 8 July, the high-salinity intensity of the eddy generally decreased except for the increases on 27 June. In the second stage, from 13 to 29 July, there was a remarkable rise in the high-salinity intensity

coast of Luzon Island in this saline environment on 20 June. Saline Kuroshio water was effectively trapped within the eddy during its generation (Figure 13b). The eddy then propagated northwestward (Figure 13c), gradually separating from the Kuroshio and with its salinity decaying, representing the first stage. During the second stage, the AE remained southwest of Taiwan for about 2 weeks (Figure 13d), and then turned to propagate westward (Figure 13e). During this stage, a significant saline Kuroshio water mass appeared in the Luzon Strait, introducing a large additional component of saline water onto the southeast fringe of the eddy. The eddy was first zonally stretched and then induced a large saline Kuroshio intrusion (Figures 13e and 13f). The westward eddy flows on its southern fringe conveyed the saline water westward (Figure 13e), and more saline water was incorporated into the eddy as it propagated (Figure 13f). In the following 20 days until early August, saline water was continuously absorbed into the eddy, but the intensity weakened (Figure 13g). This was followed by a period of decay (Figures 13h and 13i). The connection between the AE and the Kuroshio was broken because the zonal radius of the eddy was reduced. As the supply of saline water was cut off, the high-salinity water within the eddy mixed away rapidly.

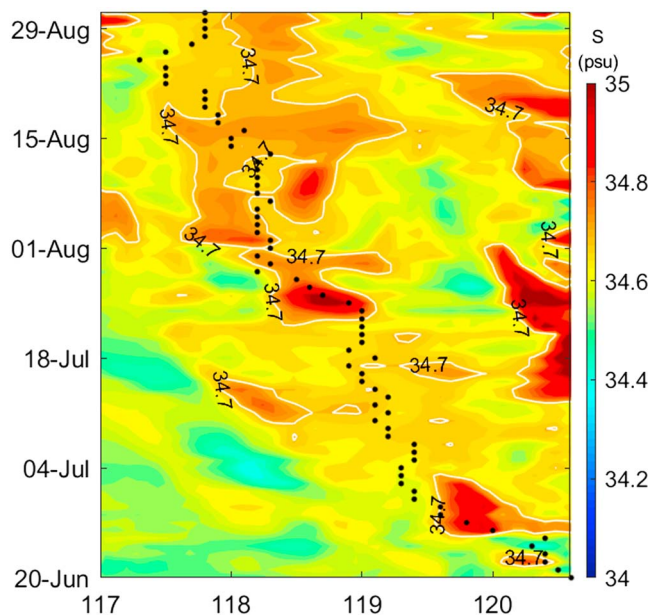


Figure 11. Time-longitude distribution of daily subsurface salinity (at 200-m depth) along 21°N. The black dots are eddy centers at the same time. The white lines show the 34.70-psu isohaline.

4.3. Salinity Balance Diagnosis

The two stages are different and may have been modulated by different dynamic processes. A simplified salt budget has been diagnosed to

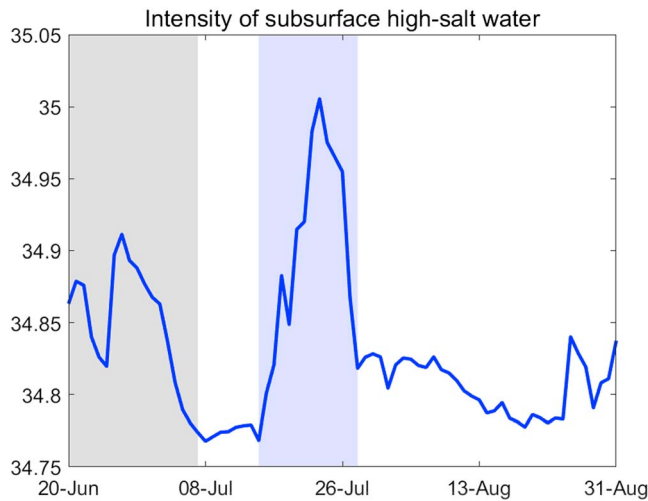


Figure 12. High-salinity intensity (I_s) of the eddy in the subsurface (at 200-m depth). The gray and blue shading represent the two stages of eddy-induced salt transport.

understand the dynamics of the saline Kuroshio water intrusion. Consistent with the above discussion, the first stage was dominated by a negative salinity tendency (Figure 14a). Advection partly contributed to the salinity decay (Figure 14b). Saline Kuroshio water was already incorporated within the AE when it formed. As the AE separated from the Kuroshio and propagated northwestward, the supply of saline water was shut down, which led to the decrease in salinity (Figure 12). The spatial field of the horizontal advection shows strong positive salinity advection west of the eddy center, but negative salinity advection east of the center (Figure 15a). Note that the effect of horizontal advection cannot fully explain the decrease in subsurface salinity. In addition to the vertical mixing term that was omitted due to the lack of data, the turbulent mixing around the eddy boundary caused by the large salinity gradient between the saline Kuroshio water within the eddy and the surrounding fresh NSCS water is likely to induce strong salinity mixing due to shear instability (Jing et al., 2011; Yang et al., 2014).

During the second stage, the salinity budget shows that the positive subsurface salinity tendency was mainly supported by the horizontal advection term (Figure 14). The advection contributes more than 75% of the subsurface salinity increase. The spatial distribution of subsurface salinity and the horizontal advection term also show the important contribution of advection to the salinity increases (Figures 14b and 15b). In this

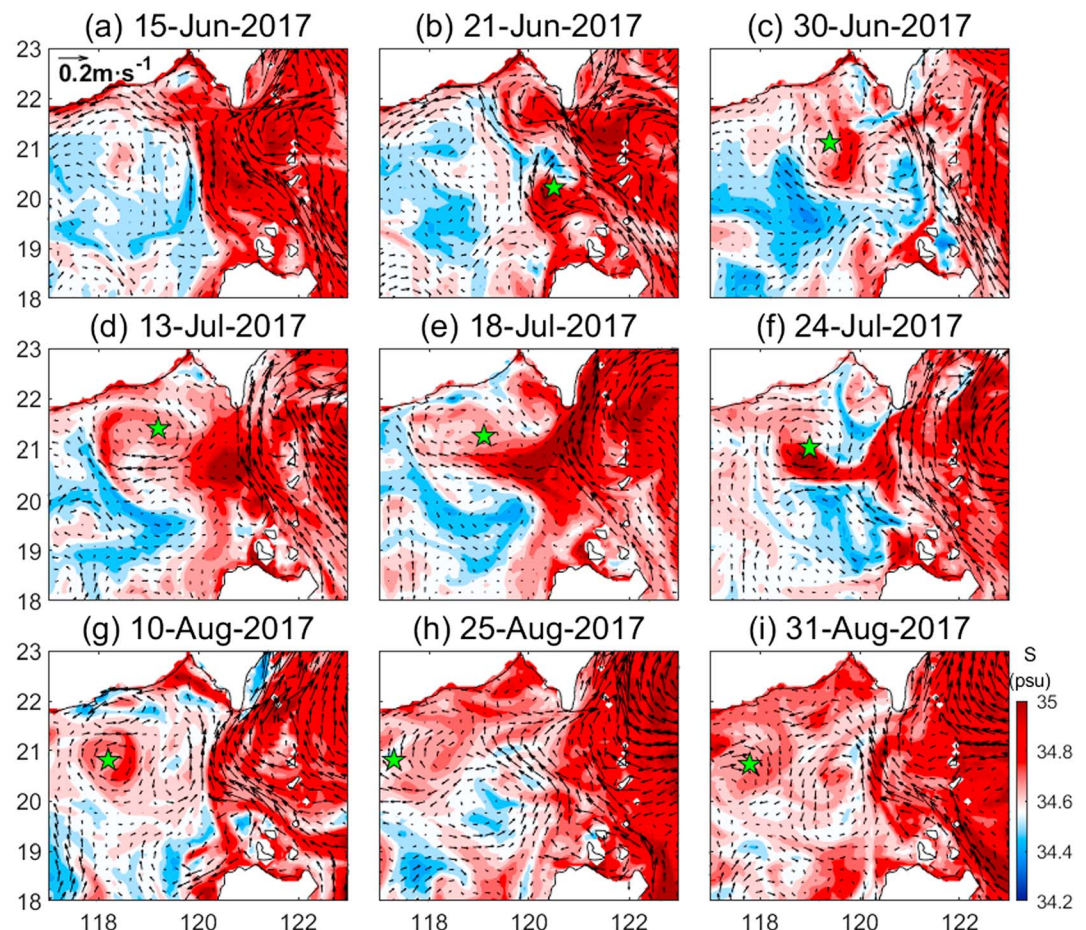


Figure 13. Evolution of salinity (shading; units: psu) and ocean currents (vectors; units: m/s) in the subsurface (200-m depth). The green stars are the corresponding eddy centers.

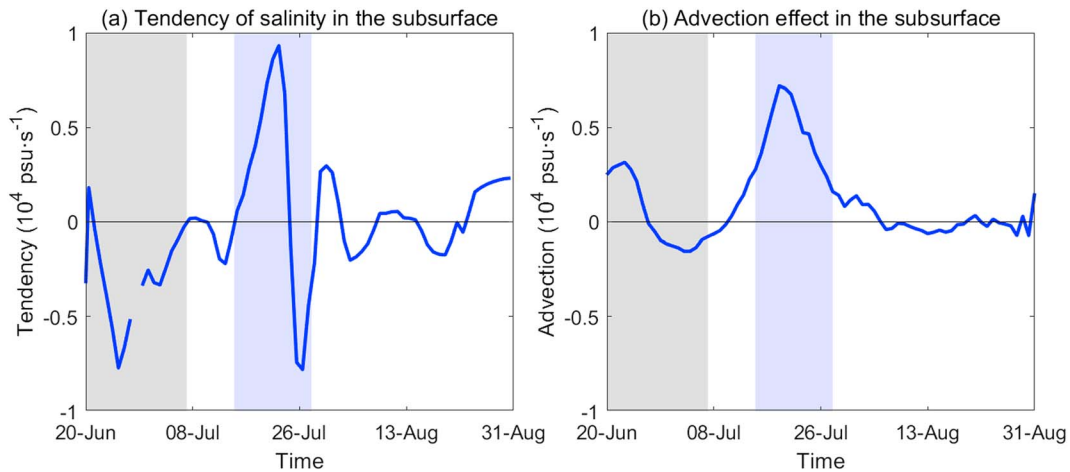


Figure 14. (a) Salinity tendency (units: psu/s) within the eddy (defined on a $1^\circ \times 1^\circ$ bin around the eddy center in the first stage and then expanded to $2^\circ \times 2^\circ$) in the subsurface (at 200-m depth). (b) Salinity advection (units: psu/s) within the eddy box in the subsurface. The gray and blue shading represent the two eddy transport stages. The salinity tendency and advection time series are standardized.

stage, the saline Kuroshio water continuously accumulates in the Luzon Strait as a result of the Kuroshio intrusion. Under favorable conditions, the southern fringe of the zonally stretched AE conveys abundant saline Kuroshio water into the NSCS. Note that the contribution of the salinity advection term in the second stage is much stronger than in the first stage. That is, the horizontal advection effect plays a major role in the eddy-induced intrusion of saline Kuroshio water, especially for the second stage.

As detailed in section 2.3, the total advection term can be divided into two parts: salt advection by mean flow and by eddy currents (equation (2)). To quantitatively evaluate their relative importance, these two components are shown in Figure 16. The effect of the mean flow is generally to reduce the salinity (Figure 16a). In contrast, the eddy advection tends to intensify the salinity and induces the advection peak during the second stage (Figure 16b). The eddy advection effect dominates the salinity advection term, accounting for about 75% (Figures 14b and 16b). This confirms that the saline Kuroshio water can be conveyed into the NSCS by mesoscale eddies due to the eddy advection effect.

5. Discussion

This study provides important evidence for the eddy transport of saline Kuroshio water into the NSCS. It also confirms that the mesoscale eddies play an important role in the exchange of heat and water through the Luzon Strait. Su (2004) reported that at least 7–8 anticyclonic eddies are needed each year to contribute a 4.2–5.0 Sv transport into the SCS through the Luzon Strait. The mesoscale eddies that are shed from the

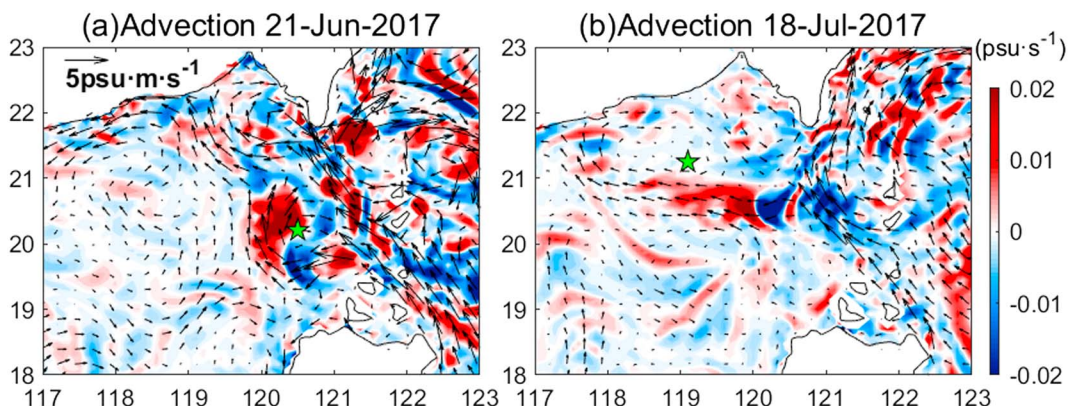


Figure 15. (a) Typical snapshots of the salinity advection term (shading; unit: psu/s) and salt flux (vectors; unit: $\text{psu}\cdot\text{m/s}$) on 21 June. (b) Same as (a) but for 18 July. The green stars are eddy centers.

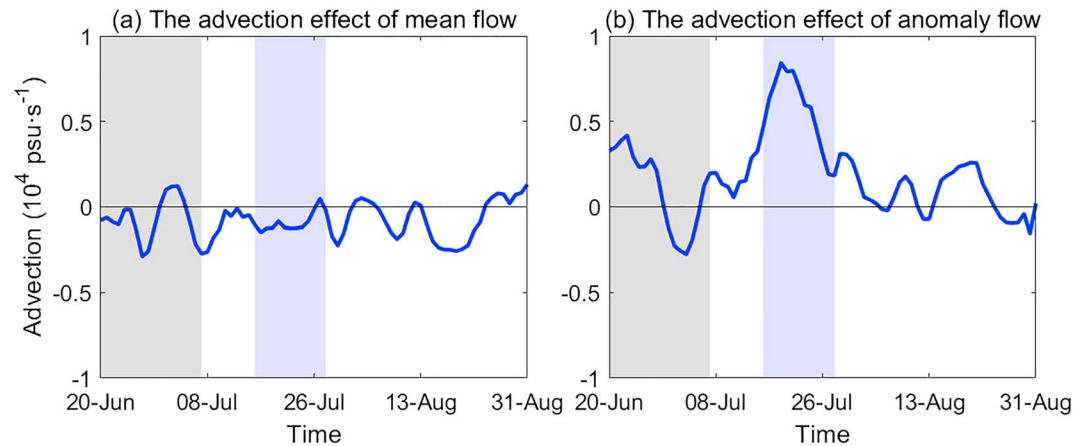


Figure 16. Salinity advection effect of (a) the mean flow and (b) eddy flow within the eddy region in the subsurface (at 200-m depth). The gray and blue shading represent the two eddy-induced salt transport stages.

Kuroshio can convey saline water into the SCS due to its self-contained saline water. This corresponds to the first stage of transport by the AE identified in this study.

Based on the typical eddy case, the annual mean and total heat, salt, and volume transports induced by eddies shed from the Kuroshio have been estimated. Using two reconstructed cases of cyclonic and anticyclonic eddies, Wang et al. (2012) estimated the annual mean eddy-induced heat, salt, and volume transport by 26 cyclonic eddies and 12 anticyclonic eddies in the vicinity of the Luzon Strait as $(3 \pm 1) \times 10^{-5}$ PW, $(4 \pm 1) \times 10^{-5}$ kg/s and 0.3 Sv, respectively. Similarly, based on observations of a typical AE, Zhang et al. (2017) indicated that the total salinity transport by 19 prominent Kuroshio Loop Current eddies from 1992 to 2014 contributed 6.8–10.8% of the upper-layer Luzon Strait transport into the SCS.

The question arises as to whether the total or mean transport calculated from the chosen eddy cases can provide an accurate assessment of transport capacity. For example, the single eddy volume transport is estimated as 0.45×10^{13} m³ for the AE observed in this study. There still has a certain gap with Zhang et al.'s (2017) result of $0.89\text{--}1.44 \times 10^{13}$ m³. Given the diversity of eddies, taking the typical case as a calculation standard might not fully reflect the net eddy effect. To improve the evaluation of eddy-induced transport, accurate assessment of the transport using more observations of eddies is required.

In addition to the transport associated with eddies shed from the Kuroshio, this study provides important evidence for the salt transport when the eddies move away from the Kuroshio area, that is, the second transport stage. Does this mean that some locally generated eddies also have the ability to transport the Kuroshio

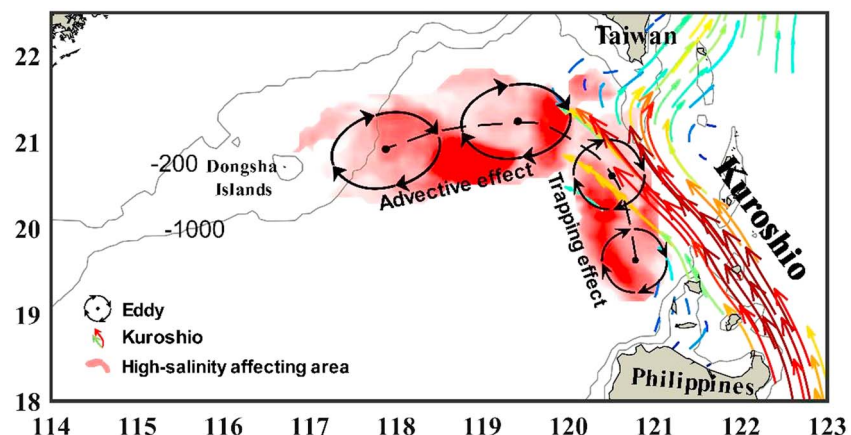


Figure 17. Schematic of the eddy-induced salinity transport described in this study. Red shading denotes the high-salinity intrusion area. The lighter (darker) shading in the high-salinity area indicates lower (higher) subsurface salinity intensity.

water into the SCS? This contribution has never been considered in the evaluation of the eddy-induced heat, salt, and mass transport. To further improve the estimate of eddy transport, more comprehensive analysis is needed.

Our companion work indeed finds that some locally formed eddies also have the capability to transport salt. From 1993 to 2018, 122 eddies shed by the Kuroshio and 69 locally generated eddies transported high-saline water into the SCS (figure not shown). Future work will include further statistical analysis of all eddies that are capable of transporting saline Kuroshio water into the SCS. Further investigation of eddy-induced salt transport will be carried out using available Argo float data, high-resolution satellite SSS measurements, and model output.

6. Conclusions

The Kuroshio carries large amounts of water mass, heat, and salt from low latitude to midlatitude into the NSCS, affecting its physical and biogeochemical properties. Observations from a targeted joint hydrographic investigation have identified significant saline Kuroshio water intrusion accompanying an AE. Details and dynamics of this eddy-induced transport were investigated using HYCOM output.

The eddy transport process consists of two stages, and the related dynamics are summarized in Figure 17. In the first stage, an AE was generated within the Kuroshio loop near the Luzon Strait, trapping large quantities of saline Kuroshio water within it. After its being shed from the Kuroshio, saline Kuroshio water dissipated, probably associated with strong salinity mixing due to shear instability between the saline AE and fresh NSCS water. The salinity dissipation process will be examined further by model experiments in future work. Using satellite observations, in situ measurements, and profiling float data, Frenger et al. (2015) identified over a million mesoscale eddy instances in the Southern Ocean from 1997 to 2010 and suggested two distinct mechanisms during eddy propagation: trapping and stirring (not completely independent). The trapping effect for the eddy in the present study dominated in the first stage. In the second stage, the AE turned to propagate westward. Saline Kuroshio water from the Luzon Strait was conveyed to the NSCS by the eddy flow on the southern flank of the eddy, which led to a regrowth of subsurface saline water along the propagation path. The advection effect was the major mechanism of salt transport. The stirring effect is less important during the second stage than during the first.

A simplified salinity budget analysis was used to quantitatively evaluate the effect of eddy transport. The diagnostic analysis confirmed the major contribution of eddy-induced salinity advection in the salinity intrusion into the NSCS. The advection effect by eddy currents is stronger in the second stage than in the first. The simplified calculation is somewhat uncertain; for example, the vertical entrainment, detrainment, and vertical and horizontal dissipation processes are ignored, but it indeed confirms the dominant effect of eddy advection in this subsurface salt transport process. Although the quantification of a typical eddy transport process can improve the assessment of eddy-induced transport in the SCS, more comprehensive analysis is needed in future work.

References

- Bryan, K. (1996). The role of mesoscale eddies in the poleward transport of heat by the oceans: A review. *Physica D: Nonlinear Phenomena*, 98(2–4), 249–257. [https://doi.org/10.1016/0167-2789\(96\)00119-4](https://doi.org/10.1016/0167-2789(96)00119-4)
- Chassignet, E. P., Hurlburt, H. E., Smedstad, O. M., Halliwell, G. R., Hogan, P. J., Wallcraft, A. J., et al. (2007). The HYCOM (Hybrid Coordinate Ocean Model) data assimilative system. *Journal of Marine Systems*, 65(1–4), 60–83. <https://doi.org/10.1016/j.jmarsys.2005.09.016>
- Chen, G. (2010). Mesoscale eddies in the South China Sea: Mean properties and spatio-temporal variability [in Chinese]. Graduate School of Chinese Academy of Sciences (Institute of Oceanography).
- Chen, G., Gan, J., Xie, Q., Chu, X., Wang, D., & Hou, Y. (2012). Eddy heat and salt transports in the South China Sea and their seasonal modulations. *Journal of Geophysical Research*, 117, C05021. <https://doi.org/10.1029/2011JC007724>
- Chen, G., Hou, Y., & Chu, X. (2011). Mesoscale eddies in the South China Sea: Mean properties, spatiotemporal variability, and impact on thermohaline structure. *Journal of Geophysical Research*, 116, C06018. <https://doi.org/10.1029/2010JC006716>
- Chen, Y., Yu, K., Dong, C., He, Z., Yan, Y., & Wang, D. (2017). Evaluation of satellite-altimetry-derived pycnocline depth products in the South China Sea. *Remote Sensing*, 9(8), 822. <https://doi.org/10.3390/rs9080822>
- Cheney, R. E., & Richardson, P. L. (1976). Observed decay of a cyclonic gulf stream ring. *Deep Sea Research and Oceanographic Abstracts*, 23(2), 143–155. [https://doi.org/10.1016/S0011-7471\(76\)80023-X](https://doi.org/10.1016/S0011-7471(76)80023-X)
- Chu, X., Xue, H., Qi, Y., Chen, G., Mao, Q., Wang, D., & Chai, F. (2014). An exceptional anticyclonic eddy in the South China Sea in 2010. *Journal of Geophysical Research: Oceans*, 119, 881–897. <https://doi.org/10.1002/2013JC009314>

Acknowledgments

Highly detailed comments and excellent suggestions for revision from anonymous reviewers are gratefully acknowledged. We benefited from numerous freely available datasets: the AVISO dataset (<https://www.aviso.altimetry.fr>), HYCOM reanalysis output (<http://hycom.org/dataserver/glb-reanalysis>), and the SCSP0D14TempSalt climatological dataset (<https://doi.org/10.6084/m9.figshare.c.1513842>), and the XCTD observations (executed by the SCSIO, Chinese Academy of Sciences) and Sea-Wing underwater glider observations (developed and provided by Jiancheng Yu and Shuo Li from the Shenyang Institute of Automation, Chinese Academy of Sciences; <https://zenodo.org/record/3365885>). This research was supported by the National Natural Science Foundation of China (41521005) and the National Natural Science Foundation of China (41776025, 41606030, 41776026, and 41676018). Q. W. is sponsored by the Pearl River S&T Nova Program of Guangzhou (201906010051). Y. W. is sponsored by Open Foundation of Key Laboratory of Technology for Safeguarding of Maritime Rights and Interests and Application, SOA (SCS1616).

- Dong, C., McWilliams, J. C., Liu, Y., & Chen, D. (2014). Global heat and salt transports by eddy movement. *Nature Communications*, 5(1), 3294. <https://doi.org/10.1038/ncomms4294>
- Evans, R. H., Baker, K. S., Brown, O. B., & Smith, R. C. (1985). Chronology of Warm-Core Ring. *Journal of Geophysical Research*, 90(C5), 8803–8811. <https://doi.org/10.1029/JC090iC05p08803>
- Frenger, I., Münnich, M., Gruber, N., & Knutti, R. (2015). Southern Ocean eddy phenomenology. *Journal of Geophysical Research: Oceans*, 120, 7413–7449. <https://doi.org/10.1002/2015JC011047>
- Gordon, A. L., Huber, B. A., Metzger, E. J., Susanto, R. D., Hurlburt, H. E., & Adi, T. R. (2012). South China Sea throughflow impact on the Indonesian throughflow. *Geophysical Research Letters*, 39, L11602. <https://doi.org/10.1029/2012GL052021>
- Hetland, R. D., Hsueh, Y., Leben, R. R., & Niiler, P. P. (1999). A loop current-induced jet along the edge of the West Florida Shelf. *Geophysical Research Letters*, 26(15), 2239–2242. <https://doi.org/10.1029/1999GL900463>
- Huang, Q. Z. (1992). General situations of the current and eddy in the South China Sea. *Advance in Earth Sciences*, 7(5), 1–9.
- Hurlburt, H. E., & Thompson, J. D. (1980). A numerical study of loop current intrusions and eddy shedding. *Journal of Physical Oceanography*, 10(10), 1611–1651.
- Jayne, S. R., & Marotzke, J. (2002). The oceanic eddy heat transport. *Journal of Physical Oceanography*, 32(32), 3328–3345.
- Jia, Y., & Liu, Q. (2004). Eddy Shedding from the Kuroshio Bend at Luzon Strait. *Journal of Oceanography*, 60(6), 1063–1069.
- Jing, Z., Wu, L., Li, L., Liu, C., Liang, X., Chen, Z., et al. (2011). Turbulent diapycnal mixing in the subtropical northwestern pacific: Spatial-seasonal variations and role of eddies. *Journal of Geophysical Research*, 116, C10028. <https://doi.org/10.1029/2011JC007142>
- Lee, M. M., Marshall, D. P., & Williams, R. G. (1997). On the eddy transfer of tracers: advective or diffusive? *Journal of Marine Research*, 55(3), 483–505. <https://doi.org/10.1357/0022240973224346>
- Lee, M. M., Nurser, A. J. G., Coward, A. C., & de Cuevas, B. A. (2007). Eddy advective and diffusive transports of heat and salt in the southern ocean. *Journal of Physical Oceanography*, 37(5), 1376–1393. <https://doi.org/10.1175/JPO3057.1>
- Li, L., Nowlin, W. D. Jr., & Su, J. (1998). Anticyclonic rings from the Kuroshio in the South China Sea. *Deep Sea Research Part I Oceanographic Research Papers*, 45(9), 1469–1482. [https://doi.org/10.1016/S0967-0637\(98\)00026-0](https://doi.org/10.1016/S0967-0637(98)00026-0)
- Li, Y., & Wang, F. (2012). Spreading and salinity change of North Pacific Tropical Water in the Philippine Sea. *Journal of Oceanography*, 68(3), 439–452. <https://doi.org/10.1007/s10872-012-0110-3>
- Lin, Y. C., Oey, L. Y., Wang, J., & Liu, K. K. (2015). Rossby waves and eddies observed at a temperature mooring in northern South China Sea. *Journal of Physical Oceanography*. <https://doi.org/10.1175/JPO-D-15-0094.1>
- Liu, Y., Dong, C., Guan, Y., Chen, D., McWilliams, J., & Nencioli, F. (2012). Eddy analysis in the subtropical zonal band of the North Pacific Ocean. *Deep-Sea Research Part I*, 68(5), 54–67. <https://doi.org/10.1016/j.dsr.2012.06.001>
- McWilliams, J. C., & Flierl, G. R. (1979). On the evolution of isolated, nonlinear vortices. *Journal of Physical Oceanography*, 9(6), 1155–1182. [https://doi.org/10.1175/1520-0485\(1979\)009<1155:OTEOIN>2.0.CO;2](https://doi.org/10.1175/1520-0485(1979)009<1155:OTEOIN>2.0.CO;2)
- Nan, F., He, Z., Zhou, H., & Wang, D. (2011). Three long-lived anticyclonic eddies in the northern South China Sea. *Journal of Geophysical Research*, 116, C05002. <https://doi.org/10.1029/2010JC006790>
- Nan, F., Yu, F., Xue, H., Wang, R., & Si, G. (2015). Ocean salinity changes in the northwest pacific subtropical gyre: The quasi-decadal oscillation and the freshening trend. *Journal of Geophysical Research: Oceans*, 120, 2179–2192. <https://doi.org/10.1002/2014JC010536>
- Qu, T., Du, Y., & Sasaki, H. (2006). South China Sea throughflow: A heat and freshwater conveyor. *Geophysical Research Letters*, 33, L23617. <https://doi.org/10.1029/2006GL028350>
- Qu, T., Mitsudera, H., & Yamagata, T. (2000). Intrusion of the North Pacific waters into the South China Sea. *Journal of Geophysical Research*, 105(C3), 6415–6424. <https://doi.org/10.1029/1999JC900323>
- Sadarjoen, I. A., & Post, F. H. (2000). Detection, quantification, and tracking of vortices using streamline geometry. *Computers & Graphics*, 24(3), 333–341. [https://doi.org/10.1016/S0097-8493\(00\)00029-7](https://doi.org/10.1016/S0097-8493(00)00029-7)
- Sangrà, P., Pelegrí, J. L., Hernández-Guerra, A., Arregui, I., Martín, J. M., Marrero-Díaz, A., et al. (2005). Life history of an anticyclonic eddy. *Journal of Geophysical Research*, 110, C03021. <https://doi.org/10.1029/2004JC002526>
- Schultz Tokos, K. L., Hinrichsen, H. H., & Zenk, W. (1994). Merging and migration of two eddies. *Journal of Physical Oceanography*, 24(10), 2129–2141. [https://doi.org/10.1175/1520-0485\(1994\)024<2129:MAMOTM>2.0.CO;2](https://doi.org/10.1175/1520-0485(1994)024<2129:MAMOTM>2.0.CO;2)
- Sheu, W. J., Wu, C. R., & Oey, L. Y. (2010). Blocking and westward passage of eddies in the Luzon Strait. *Deep Sea Research Part II: Topical Studies in Oceanography*, 57(19–20), 1783–1791. <https://doi.org/10.1016/j.dsr.2010.04.004>
- Shu, Y., Chen, J., Li, S., Wang, Q., Yu, J., & Wang, D. (2018). Field-observation for an anticyclonic mesoscale eddy consisted of twelve gliders and sixty-two expendable probes in the northern South China Sea during summer 2017. *Science China Earth Sciences*, 62, 451–458.
- Shu, Y., Xue, H., Wang, D., Chai, F., Xie, Q., Yao, J., & Xiao, J. (2014). Meridional overturning circulation in the South China Sea envisioned from the high-resolution global reanalysis data GLBa0.08. *Journal of Geophysical Research: Oceans*, 119, 3012–3028. <https://doi.org/10.1002/2013JC009583>
- Su, J. (2004). Overview of the South China Sea circulation and its influence on the coastal physical oceanography outside the pearl river estuary. *Continental Shelf Research*, 24(16), 1745–1760. <https://doi.org/10.1016/j.csr.2004.06.005>
- Su, J., Xu, J. P., Cai, S. Q., & Wang, Q. (1999). *Gyres and eddies in the South China Sea, in Onset and evolution of the South China Sea monsoon and its interaction with the ocean [in Chinese]*. Beijing: China Meteorol. Press.
- Volkov, D. L., Tong, L., & Fu, L. (2008). Eddy-induced meridional heat transport in the ocean. *Geophysical Research Letters*, 35, L20601. <https://doi.org/10.1029/2008GL035490>
- Wang, D., Liu, Q., Huang, R. X., Du, Y., & Qu, T. (2006). Interannual variability of the South China Sea throughflow inferred from wind data and an ocean data assimilation product. *Geophysical Research Letters*, 33, L14605. <https://doi.org/10.1029/2006GL026316>
- Wang, D., Xu, H., Lin, J., & Hu, J. (2008). Anticyclonic eddies in the northeastern South China Sea during winter 2003/2004. *Journal of Oceanography*, 64(6), 925–935. <https://doi.org/10.1007/s10872-008-0076-3>
- Wang, G., Su, J., & Chu, P. C. (2003). Mesoscale eddies in the South China Sea observed with altimeter data. *Geophysical Research Letters*, 30(21), 2121. <https://doi.org/10.1029/2003GL018532>
- Wang, L., Koblinsky, C. J., & Howden, S. (2000). Mesoscale variability in the South China Sea from the TOPEX/Poseidon altimetry data. *Deep-Sea Research Part I*, 47(4), 681–708. [https://doi.org/10.1016/S0967-0637\(99\)00068-0](https://doi.org/10.1016/S0967-0637(99)00068-0)
- Wang, Q., Zeng, L., Zhou, W., Xie, Q., Cai, S., Yao, J., & Wang, D. (2014). Mesoscale eddies cases study at Xisha waters in the South China Sea in 2009/2010. *Journal of Geophysical Research: Oceans*, 120, 517–532. <https://doi.org/10.1002/2014JC009814>
- Wang, X., Li, W., Qi, Y., & Han, G. (2012). Heat, salt and volume transports by eddies in the vicinity of the Luzon Strait. *Deep-Sea Research Part I*, 61, 21–33. <https://doi.org/10.1016/j.dsr.2011.11.006>
- Waterman, S. N. (2009). Eddy-mean flow interactions in western boundary current jets, DOI: <https://doi.org/10.1575/1912/2832>.

- Xiao, F., Zeng, L., Liu, Q. Y., Zhou, W., & Wang, D. (2017). Extreme subsurface warm events in the South China Sea during 1998/99 and 2006/07: Observations and mechanisms. *Climate Dynamics*, *50*(1-2), 115–128.
- Xiu, P., Chai, F., Shi, L., Xue, H., & Chao, Y. (2010). A census of eddy activities in the South China Sea during 1993–2007. *Journal of Geophysical Research*, *115*, C03012. <https://doi.org/10.1029/2009JC005657>
- Yang, Q., Zhao, W., Li, M., & Tian, J. (2014). Spatial structure of turbulent mixing in the northwestern Pacific Ocean. *Journal of Physical Oceanography*, *44*(8), 2235–2247. <https://doi.org/10.1175/JPO-D-13-0148.1>
- Zeng, L., Chassignet, E. P., Schmitt, R. W., Xu, X., & Wang, D. (2018). Salinification in the South China Sea since late 2012: A reversal of the freshening since the 1990s. *Geophysical Research Letters*, *45*, 2744–2751. <https://doi.org/10.1002/2017GL076574>
- Zeng, L., Liu, W. T., Xue, H., Xiu, P., & Wang, D. (2014). Freshening in the South China Sea during 2012 revealed by Aquarius and in situ data. *Journal of Geophysical Research: Oceans*, *119*, 8296–8314. <https://doi.org/10.1002/2014JC010108>
- Zeng, L., Wang, D., Chen, J., Wang, W., & Chen, R. (2016). SCSP0D14, a South China Sea physical oceanographic dataset derived from in situ measurements during 1919–2014. *Scientific Data*, *3*(1), 160029. <https://doi.org/10.1038/sdata.2016.29>
- Zeng, L., Wang, D., Xiu, P., Shu, Y., Wang, Q., & Chen, J. (2016). Decadal variation and trends in subsurface salinity from 1960 to 2012 in the northern South China Sea. *Geophysical Research Letters*, *43*, 12,181–12,189. <https://doi.org/10.1002/2016GL071439>
- Zhang, F. (1994). Diagnostic calculations for the seasonal-averaged current field in the deep water zone of the South China Sea. *Tropic Oceanology*, *13*, 8–16.
- Zhang, Z., Wang, W., & Qiu, B. (2014). Oceanic mass transport by mesoscale eddies. *Science*, *345*(6194), 322–324. <https://doi.org/10.1126/science.1252418>
- Zhang, Z., Zhao, W., Qiu, B., & Tian, J. (2017). Anticyclonic eddy sheddings from Kuroshio Loop and the accompanying cyclonic eddy in the northeastern South China Sea. *Journal of Physical Oceanography*, *47*(6), 1243–1259. <https://doi.org/10.1175/JPO-D-16-0185.1>